Math. Model. Nat. Phenom.
Vol. 3, No. 1, 2008, pp. 98-107

Scale Dependence of Contact Line Computations

O. Weinstein[a] and L.M. Pismen[a,b,1]

[a] Department of Chemical Engineering, Technion, 32000 Haifa, Israel
[b] Minerva Center for Nonlinear Physics of Complex Systems, Technion, 32000 Haifa, Israel

Abstract. The shape and velocity of a sliding droplet are computed by solving the Navier–Stokes equation with free interface boundary conditions. The Galerkin finite element method is implemented in a 2D computation domain discretized using an unstructured mesh with triangular elements. The mesh is refined recursively at the corners (contact points). The stationary sliding velocity is found to be strongly dependent on grid refinement, which is a consequence of the contact line singularity resolved through the effective slip across the finite elements adjacent to the contact point. For small droplets, this dependence is well approximated by a theoretical estimates obtained using multiscale expansion and matching technique in lubrication approximation, where the corner element size is used as a microscale parameter. For larger droplets, the shape is also dependent on grid refinement. This questions the validity of numerous computations of flows with moving contact line where grids are invariably much more coarse than molecular scales on which the singularity is resolved. It is suggested that extrapolation to molecular scales should be used to obtain realistic results.

Key words: contact line, finite elements, slip
AMS subject classification: 76D05, 76D45, 68-04

1 Introduction

It is well known that dynamic computations of a three-phase contact line are plagued by the non-integrable singularity of the classical hydrodynamic description [1, 2]. The singularity is usually alleviated in fluid-mechanical computations by introducing effective slip at the solid surface in the vicinity of the three-phase boundary and using an empirical velocity

[1]Corresponding author. Email: pismen@technion.ac.il

Article available at http://www.mmnp-journal.org or http://dx.doi.org/10.1051/mmnp:2008035

dependence of the dynamic contact angle. This approach has been usually implemented in the framework of lubrication approximation (for review, see Ref. [3]). Computational aspects of slip models were recently reviewed by Shikhmurzaev [4]. Other approaches include taking into account a thin precursor layer which may form even under conditions of partial wetting [5, 6, 7], diffuse interface computations [8, 9] and postulating special rheological properties of the liquid-vapor interface in the contact line region [10].

On a macroscopic level, the distinction between different physical models is blurred, since all of them bring about in the framework of perturbation theories a logarithmic factor containing the ratio of a macroscopic and microscopic length with a model-dependent coefficient [11, 12]. In all physical models the microscopic length, be it the precursor layer thickness, diffuse interface thickness or slip length, is related to molecular interactions and lies in or below nanometer range. Since numerical routines are all but impossible to implement for realistic ratios of many orders of magnitude, the singularity cannot be resolved on a physically relevant scale in practical computations, which are all restricted to moderate scale ratios.

The dependence on grid size is rarely brought to attention, though it was detected in recent computations of curtain coating [13]. It should be emphasized that, owing to the contact line singularity, this dependence never saturates, unless near-molecular resolution is reached. The aim of this communication is to demonstrate the essential scale dependence of contact line computations by applying grid refinement near the singular point.

2 Basic Equations

As a test problem, we take a standard case of a droplet sliding along an inclined plane. The problem is reduced to a dimensionless form, where the spatial coordinates $\mathbf{x} = (x, y)$ are scaled by the length d of the footprint of a quiescent droplet, and the flow velocity $\mathbf{u}$ is scaled by $u^* = \rho g d^2/\mu$, where ρ is the fluid density, μ is dynamic viscosity, and g is acceleration of gravity; the time scale is d/u^*, and the pressure p is scaled by $\mu u^*/d$. In this formulation, the solution depends on two angles – the inclination angle α and is the static contact angle θ – and two dimensionless parameters – the Reynolds number $\mathrm{Re} = \rho u^* d/\mu = \rho^2 d^3 g/\mu^2$ and the capillary number $\mathrm{Ca} = \mu u^*/\gamma$, where γ is surface tension. In addition, the solution depends, as we shall see, on the discretization scale that determines the slip near the contact line. Note that the adopted velocity scale, though convenient for formulating the problem, is much larger than actual velocity of a sliding droplet; this is the reason why nominal Reynolds numbers in the examples below are very large, while dimensionless velocities are small.

We solve the standard Navier–Stokes and continuity equations for an incompressible Newtonian fluid written in the dimensionless form

$$\mathrm{Re}\left(\frac{\partial \mathbf{u}}{\partial t} + \mathbf{u}\cdot\nabla\mathbf{u}\right) = -\nabla p + \nabla^2\mathbf{u} + \mathbf{g}, \quad \nabla\cdot\mathbf{u} = 0, \tag{2.1}$$

where $\mathbf{g}$ is the unit vector in the direction of gravity. The normal and tangential stress

balance boundary conditions on the free interface Γ (neglecting air viscosity) are

$$p - \mathbf{n} \cdot \left[\nabla \mathbf{u} + \nabla \mathbf{u}^T\right] \cdot \mathbf{n} = K\mathrm{Ca}^{-1}, \quad \mathbf{n} \cdot \left[\nabla \mathbf{u} + \nabla \mathbf{u}^T\right] \cdot \mathbf{t} = 0. \tag{2.2}$$

where $\mathbf{n}$, $\mathbf{t}$ are unit vectors normal and tangential to the free interface, $K = d\mathbf{t}/ds$ is interfacial curvature, s is the arc length. The boundary condition on the substrate is the standard no-slip condition $\mathbf{u} = 0$. The singularity at the contact line is, however, avoided due to numerical slip. In order to emphasize dependence of the results on the grid size, we do not introduce additional slip, which in any case would involve, for physically realistic values, lengths far beyond feasible precision of macroscopic computations.

3 Numerical Method

The numerical solution is obtained using the Galerkin finite element method, with the boundary conditions implemented following the procedure described in Ref. [15]. The 2D computation domain is discretized using an unstructured mesh with triangular elements, each comprising six velocity nodes and three pressure nodes. A sample mesh is shown in Fig. 1a. The mesh is further refined recursively at the corners (contact points) as shown in Fig. 1b.

The discretized version of Eqs. (2.1) is weighted by global basis functions $N_i \quad (i = 1, ..., n)$, $L_i, \quad (i = 1, ..., l)$, where n is the number of velocity nodes and l is the number of pressure nodes, and integrated over the entire domain Ω, yielding a set of nonlinear residual algebraic equations for the velocity and pressure fields. In order to reduce the continuity requirements for the interpolation functions N_i, some terms are transformed using the Gauss theorem, bringing these equations to the form

$$\begin{aligned} R_i(\mathbf{u}) &= \int_\Omega \left[\left(\mathrm{Re}\left(\frac{\partial \mathbf{u}}{\partial t} + \mathbf{u} \cdot \nabla \mathbf{u}\right) - \mathbf{g}\right] N_i - p\nabla N_i + \left[\nabla \mathbf{u} + \nabla \mathbf{u}^T\right] \cdot \nabla N_i\right) d\Omega \\ &+ \int_\Gamma N_i \left(p\ \mathbf{n} - \left[\nabla \mathbf{u} + \nabla \mathbf{u}^T\right] \cdot \mathbf{n}\right) d\Gamma = 0. \end{aligned} \tag{3.3}$$

The boundary conditions on the substrate are imposed by replacing the appropriate finite element equations (3.3) by the statements specifying the desired value of velocity of the node (e.g. $\mathbf{u}_i = 0$). The boundary conditions on the free surface are expressed by rewriting the boundary integral in Eq. (3.3) and using the normal and tangential stress conditions (2.2), leading (in 2D) to the discretized form

$$\begin{aligned} \int_\Gamma N_i \left(p\ \mathbf{n} - \left[\nabla \mathbf{u} + \nabla \mathbf{u}^T\right] \cdot \mathbf{n}\right) d\Gamma = \int_\Gamma N_i \left(p - \mathbf{n} \cdot \left[\nabla \mathbf{u} + \nabla \mathbf{u}^T\right] \cdot \mathbf{n}\right) \cdot \mathbf{n}\ d\Gamma + \\ \int_\Gamma N_i \left(-\mathbf{t} \cdot \left[\nabla \mathbf{u} + \nabla \mathbf{u}^T\right] \cdot \mathbf{n}\right) \cdot \mathbf{t}\ d\Gamma = \frac{1}{\mathrm{Ca}} \int_\Gamma \frac{\partial N_i}{\partial s} \mathbf{t}\ d\Gamma. \end{aligned} \tag{3.4}$$

The last term in this equation has been transformed by integrating by parts.

(a)

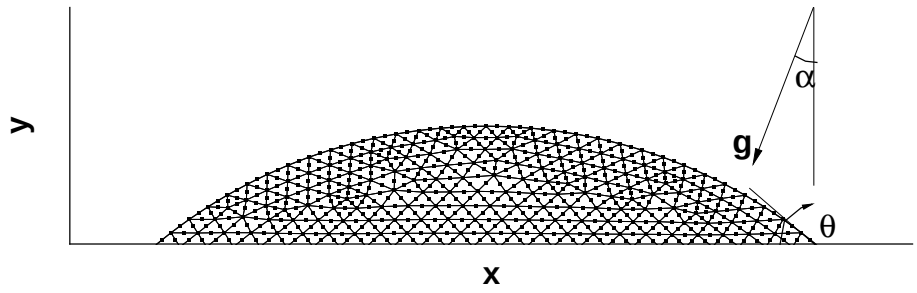

(b)

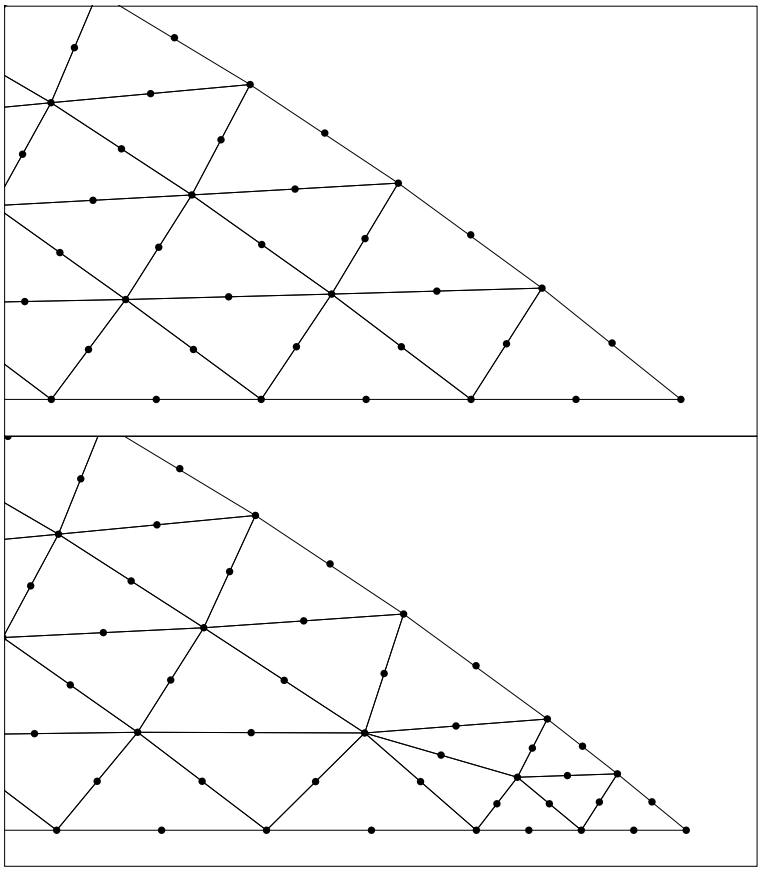

Figure 1: (a) A sample two–dimensional unstructured mesh used for droplet motion simulations; x, y are the coordinate axes; the arrow shows the direction of the gravity vector $\mathbf{g}$, α is the surface inclination angle, θ is the contact angle. (b) Scheme of mesh refinement at the contact point.

Following Ref. [14], the time derivative at a fixed location in Eq. (2.1) is transformed to the time derivative the moving mesh (denoted by an overdot):

$$\frac{\partial \mathbf{u}}{\partial t} = \dot{\mathbf{u}} - \dot{\mathbf{r}} \cdot \nabla \mathbf{u}, \tag{3.5}$$

where $\dot{\mathbf{r}}$ represents the mesh velocity. Both $\dot{\mathbf{r}}$ and $\dot{\mathbf{u}}$ are calculated using a simple backward finite difference scheme. After computing the velocity field (at time step labeled by the index $m-1$), the normal velocities at free interface nodes $\mathbf{u}_n = \mathbf{u} \cdot \mathbf{n}$ are calculated, and the new interface position (at a time step labelled by the index m) is obtained. Following this, the velocity field is recomputed for the shifted interface position, and the interface velocities updated until the calculation becomes self-consistent within the prescribed error margin of 10^{-6} in dimensionless velocity. This requires between 2 and 5 iterations at each time step.

This method can be defined as semi-implicit, since the interface displacement depends on the interfacial velocity at the end of the iterative process at each time step (m). At each time step, mesh relaxation is performed to fit the mesh to the new boundary. The contact line is translated at each time step following the displacement of interface nodes to preserve a fixed value of the contact angle at the substrate computed using a three-node approximation of the free interface. Although the shape of the last corner element remains self-similar upon attenuation due to the condition of constant true contact angle, the original corner element is reshaped as it is refined at successive iterations, so that an "apparent" contact angle at the distance equal to the original grid size slightly increases at the advancing and decreases at the receding edge.

4 Sliding Drop

Transient computations of a droplet sliding along an inclined plane are carried out taking as initial condition a stationary drop with a prescribed static contact angle θ_0 on horizontal substrate (Fig. 1). In order to avoid inertial effects causing spurious oscillations at the initial stage, the inclination slope α is increased linearly with time until the prescribed value is reached; this stage lasts about 10 % of the computation time. Following this, the computation continues with the tilt remaining constant until a steady state is attained. The calculations are then repeated at successive stages of grid refinement with the stationary shape at a preceding computation taken as the initial condition.

For small droplets, the stationary shape is perturbed only slightly, but the stationary velocity exhibits nevertheless strong dependence on grid refinement, which is a consequence of the contact line singularity resolved through the effective slip across the finite elements adjacent to the contact point. In fact, the slip is significant only in the last element. We have checked in a separate computation that the result does not change when the grid is refined uniformly throughout the computation domain. The size of the maximally refined corner element can be used therefore as a "microscale" parameter for contact line motion to compare the computational results with theoretical estimates.

The theory based the lubrication approximation on and exploring multiscale expansion and matching technique applicable at Ca $\ll 1$ [11, 17] predicts logarithmic dependence of the droplet velocity on the ratio d/λ of the characteristic macroscopic and microscopic lengths. Applying this method to the 2D model with the contact line singularity resolved through the Navier slip condition with the slip length λ, the droplet velocity is obtained as the ratio of the gravity force proportional to the droplet volume, $F_0 \approx \frac{1}{6} g\rho g d^2\theta$, to the friction factor computed at $d/\lambda \gg 1$ as

$$J_0 = \frac{6\mu}{\theta} \ln \frac{\theta d}{3\lambda}. \tag{4.6}$$

We modify these expressions using the exact formula for the droplet volume

$$F = g\rho d^2 \sin\alpha \, \frac{\theta - \frac{1}{2}\sin 2\theta}{4\sin^2\theta}, \tag{4.7}$$

and the formula for the dimensionless friction factor (scaled by μ) obtained likewise without approximating the shape of the spherical segment by a parabola,

$$J = 6\left(\theta + \frac{1}{\tan\theta} \ln \frac{d\sin\theta}{c\lambda}\right), \tag{4.8}$$

where c is an adjustable numerical constant. The droplet velocity U is expressed therefore as

$$U = \frac{U_0}{J}, \qquad U_0 = \frac{g\rho d^2 \sin\alpha}{4\mu \sin^2\theta} \left(\theta - \frac{1}{2}\sin 2\theta\right). \tag{4.9}$$

The computation results are compared with the theoretical estimate (4.9) in Fig. 2. The agreement, using a single adjustable parameter c for data sets obtained at different values of Re, Ca and different contact and inclination angles is surprisingly good, which is another testimony for the resilience of lubrication approximation going far beyond its formal application range. The corrections to simpler expressions for the force and friction factor are significant only for $\theta = 40^o$.

Dynamic distortions are significant for larger drops, which acquire a characteristic "elephant inside a boa" shape, such as shown in Fig. 3a. The grid refinement affects in this case not only the speed of motion but also the shape, which becomes more spread out at the tail upon refinement. The dependence of the speed and aspect ratio d/h (where d is the footprint length and h is the maximal height) on grid refinement is shown in Fig. 3b.

The effect of slip near the contact line originates in its immediate vicinity, and spreads out to affect the global shape of a sliding droplet through standard hydrodynamic interactions. This is the reason why refining the grid near the contact line only is sufficient, and is the most effective and economic way to capture the influence of microscopic scales on macroscopic motion. Of course, the refinement slows down numerics, and four refinements implemented in our computations reduce the scale only by the factor of 16, still far from realistic scale ratios. Actual prediction of the sliding velocity and aspect ratio can be done by *extrapolating* the results to physically justified values of the microscopic length.

(a)

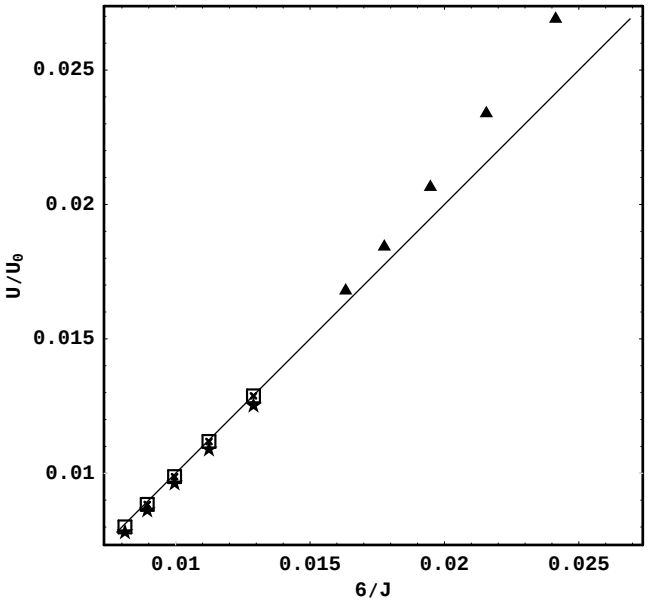

(b)

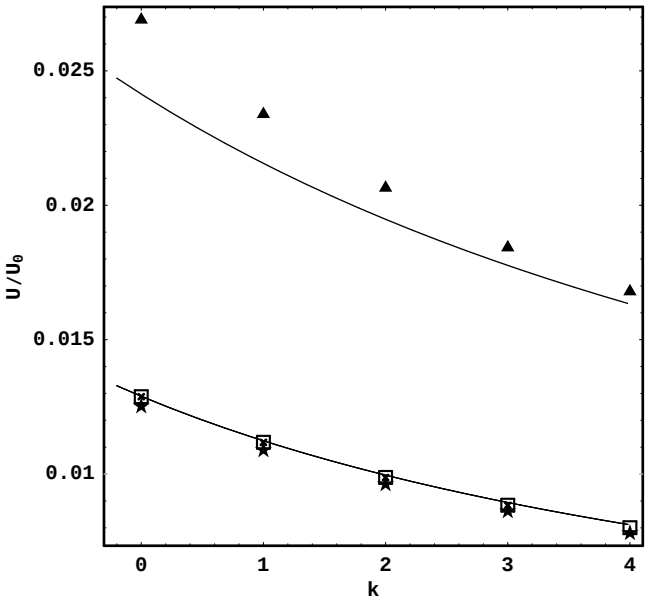

Figure 2: A comparison of numerical computation results for slowly sliding droplets with the theoretical estimate Eq. (4.9) (solid line). (a): The linear dependence of the dimensionless velocity on inverse friction factor. (b): Explicit dependence of the dimensionless velocity on the number of grid refinements k. The numerical results with four mesh refinements are given for Re = 32700, Ca = 0.308 ($d/2 = 0.7493\,mm$) $\alpha = 10^o$, $\theta = 20^o$ (squares); Re = 269000, Ca = 1.25, ($d/2 = 1.512\,mm$), $\alpha = 10^o$, $\theta = 20^o$ (stars); Re = 32700, Ca = 0.308 ($d/2 = 0.7493\,mm$), $\alpha = 40^o$, $\theta = 20^o$ (crosses); Re = 10686, Ca = 0.146 ($d/2 = 0.516\,mm$), $\alpha = 10^o$, $\theta = 40^o$ (triangles). Numbers in parentheses give the footprint length of an equivalent water droplet at 20^{o}C.

(a)

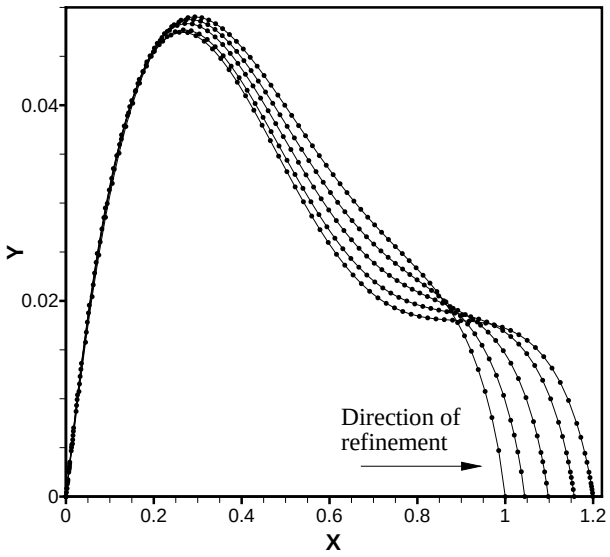

(b)

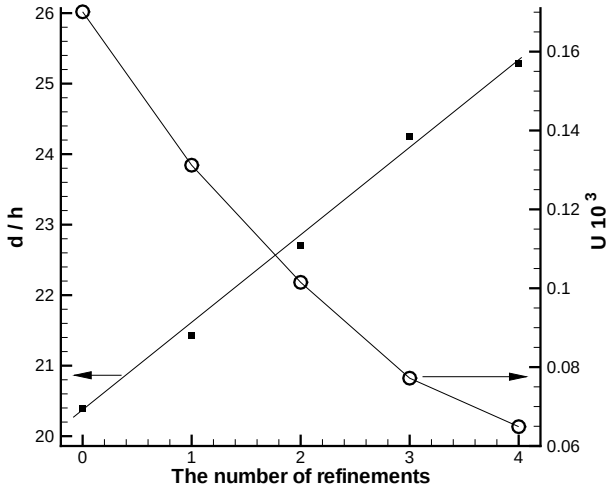

Figure 3: (a): Shapes of a sliding droplet at different refinements. The images are aligned at the advancing contact point. (b): Dependence of the speed and aspect ratio d/h on the grid refinement. Parameters: $\alpha = 40^o$, $\theta = 20^o$, $d/2 = 4.086\,mm$, Re $= 32700$, Ca $= 0.308$ (corresponding to a water droplet with $d/2 = 4.086\,mm$)

Acknowledgements

This work has been supported by Israel Science Foundation (grant 55/02).

References

[1] C. Huh, L. E. Scriven. *Hydrodynamical model of steady movement of a solid/liquid/fluid contact line.* J. Coll. Int. Sci., 35 (1971), 85.

[2] E. B. Dussan. *On the motion of a fluid-fluid interface along a solid surface.* Ann. Rev. Fluid Mech., 11 (1979), 371.

[3] A. Oron, S. G. Bankoff, S. H. Davis. *Long-scale evolution of thin liquid films.* Rev. Mod. Phys., 69 (1997), 931.

[4] Y. D. Shikhmurzaev. *Singularities at the moving contact line. Mathematical, physical and computational aspects.* Physica D: Nonlinear Phenomena, 217 (2006), 121.

[5] L. M. Pismen, Y. Pomeau. *Disjoining potential and spreading of thin liquid layers in the diffuse-interface model coupled to hydrodynamics.* Phys. Rev. E, 62 (2000), 2480.

[6] U. Thiele, M. G. Velarde, K. Neuffer, M. Bestehorn, Y. Pomeau. *Sliding drops in the diffuse interface model coupled to hydrodynamics.* Phys. Rev. E 64 (2001), 061601.

[7] L. M. Pismen. *Mesoscopic hydrodynamics of contact line motion.* Colloids and Surfaces A, 206 (2002), 11.

[8] P. Seppecher. *Moving contact lines in the Cahn–Hilliard theory.* Int. J. Engng Sci., 34 (1996), 977.

[9] D. Jacqmin. *Contact-line dynamics of a diffuse fluid interface.* J. Fluid Mech., 402 (2000), 57.

[10] Y. D. Shikhmurzaev. *Moving contact lines in liquid/liquid/solid systems.* J. Fluid Mech., 334 (1997), 211.

[11] L. M. Pismen, Y. Pomeau. *Mobility and interactions of weakly nonwetting droplets.* Phys. Fluids, 16 (2004), 2604.

[12] J. Eggers. *Contact line motion for partially wetting fluids.* Phys. Rev. E, 72 (2005), 061605.

[13] M. C. T. Wilson, J. L. Summers, Y. D. Shikhmurzaev, A. Clarke, T. D. Blake. *Nonlocal hydrodynamic influence on the dynamic contact angle: Slip models versus experiment.* Phys. Rev. E, 73 (2006), 041606.

[14] D. R. Lynch, K. O'Neill. *Continuously deforming finite elements for the solution of parabolic problems, with and without phase change.* Int. J. Num. Meth. Eng., 17 (1981), 81.

[15] K J. Ruschak. *A method for incorporating free boundaries with surface tension in finite element fluid-flow simulators.* Int. J. Num. Meth. Eng., 15 (1980), 639.

[16] B. A. Finlayson. Numerical Methods for Problems with Moving Fronts. Ravenna Park Publishing, Seattle, Washington, 1992.

[17] L.M. Pismen. *Perturbation theory for traveling droplets.* Phys. Rev. E, 74 (2006), 041605.